Cement and Concrete Research 40 (2010) 1723–1733

Contents lists available at ScienceDirect

Cement and Concrete Research

journal homepage: http://ees.elsevier.com/CEMCON/default.asp

Influence of pozzolans and slag on the microstructure of partially carbonated cement paste by means of water vapour and nitrogen sorption experiments and BET calculations

N. De Belie [a,*], J. Kratky [a], S. Van Vlierberghe [b]

[a] Magnel Laboratory for Concrete Research, Department of Structural Engineering, Ghent University, Technologiepark Zwijnaarde 904, B-9052 Ghent, Belgium
[b] Dept. of Organic Chemistry, Ghent University, Krijgslaan 281 S4, B-9000 Ghent, Belgium

ARTICLE INFO

Article history:
Received 2 December 2009
Accepted 17 August 2010

Keywords:
Microstructure (B)
Surface area (B)
Fly ash (D)
Granulated blast-furnace slag (D)
Water vapour sorption

ABSTRACT

The influence of water-to-binder ratio (0.33 to 0.50) and additions (fly ash, slag, silica fume) on the microstructure of partially carbonated cement pastes was studied by nitrogen sorption and static and dynamic water vapour sorption. The selected technique affects macropore condensation and accessibility of pores, while predrying influences removal of CSH interlayer water. BJH calculations showed the increased amount of capillary pores with higher water-to-cement ratio, and the decrease of micropores (<2 nm), in pastes with 50% or more fly ash or slag. Paste with 10% SF showed a high amount of gel pores, related to the higher amount of CSH gel, calculated from adsorption at 23% RH. A linear relation was observed between BET specific surface and water-cement ratio. Thermogravimetric analysis illustrated the influence of water-cement ratio and pozzolanic materials on the portlandite content. Introduction of silica fume, increased the specific surface accessible to water, but not to nitrogen molecules.

1. Introduction

The hydrated portland cement paste matrix is produced by the reaction of four main clinker oxide phases with water. Portland cement consists of approximately 75% by mass of C_3S and C_2S. The products of hydration of these two minerals are CSH gel and calcium hydroxide (portlandite) crystals [1]. When supplementary cementing materials or pozzolanic active material (e.g. fly ash, granulated blast furnace slag or silica fume) are present, the portlandite is consumed in a pozzolanic reaction, which also produces CSH gel [2]. The surface of fly ash, slag or silica fume also acts as thermodynamically favourable area for the formation of nuclei of hydration products. The presence of supplementary cementing materials thus has a significant influence on the microstructure of the cement matrix.

Apart from the solid hydration products, the microstructure is formed by various types of "empty space" resulting from the physico-chemical processes which are taking place during hydration of the cement paste matrix. Together with the pores introduced to concrete from other sources, this empty space can be divided into following categories [3]:

- cement matrix pores containing gel pores and capillary pores resulting from the intristic volume change of portland cement during hydration;
- pores in aggregates;
- pores formed in the transition zone between cement matrix and aggregate;
- water voids and air voids;
- cracks formed due to the stresses caused by temperature gradients and humidity changes.

According to the IUPAC recommendation the pores can be classified also based on the width as micropores (less than 2 nm), mesopores (between 2 nm and 50 nm) and macropores (larger than 50 nm). These void parts of the material are influencing a lot of important properties of concrete, like mechanical parameters, water permeability, resistance against carbonation and overall durability. Extensive research aimed at the study of the concrete porosity has been done during the past and is still appealing. This is especially valid in case of concrete containing supplementary cementing materials, like granulated blast furnace slag or fly ash. These materials, in contact with alkaline environment which is formed during the concrete hydration mainly due to the formation of calcium hydroxide, contribute to the formation of the binding phases in the matrix and thus are further influencing the resulting pore structure of the concrete [4,5].

For the characterization of pore structure of concrete, a wide variety of techniques is available, each having its field of application. Some methods, e.g. microtomography based on the observation of the sample by X-rays, can be used to characterize both open and closed pores [6]; some methods, like mercury intrusion or nitrogen adsorption, have only access to the open pores [3]. For the pore size between 2.5 nm and 100 μm the mercury intrusion porosimetry can be used, for the larger

* Corresponding author.
E-mail address: nele.debelie@ugent.be (N. De Belie).

0008-8846/$ – see front matter © 2010 Elsevier Ltd. All rights reserved.
doi:10.1016/j.cemconres.2010.08.014

pore sizes electron scanning or optical microscopy is applied; nitrogen adsorption and water vapour adsorption is used to characterize the pores mainly in the mesopore range. An exhaustive overview of the methods used for the characterization of the pore structure of concrete can be found e.g. in the book by Kalliopi [3]. Despite a lot of experimental work performed in the field of cementitious materials pore structure research, controversy still exists regarding the interpretation and relation of the results of different methods [7–9].

The work presented in this article is focused on the use of nitrogen and water vapour sorption techniques to characterize the pore structure of portland cement based pastes containing high volumes of fly ash or granulated blast furnace slag. The water vapour adsorption/desorption isotherms can be obtained experimentally using semi-equilibrium [10] or dynamic gravimetric methods [11]. Both these methods have their advantages and drawbacks. The principle of the semi-equilibrium method consists of placing the sample into a chamber with controlled temperature and humidity (e.g. desiccator filled with saturated salt solution) and then monitoring the weight change of the sample until constant weight. This method requires simple instrumentation and is often used as reference. Its drawback lies in the long time necessary to obtain results as it is necessary to wait until the near equilibrium state of the sample is reached. The explanation of this method applied on cementitious materials together with detailed information on extracting valuable information from the results can be found in Baroghel–Bouny's work [10,12].

The dynamic method is based on placing the sample in controlled temperature and humidity conditions (in this case the more usual approach to control humidity is the mixing of humid and dry gas) and continuously monitoring the weight change of the sample. The data collected can then be interlaced and extrapolated with Eq. (1), based on an analytical solution of the diffusion equation, used by several authors [11,13]:

$$m(t) = a\left(1 - be^{(-ct)}\right) \quad (1)$$

where $m(t)$ is mass of the sample at time t of the measurement and coefficients a, b and c are determined by means of non-linear curve fitting. For $t -> \infty$, thus for the system which reached the equilibrium, the $m_{eq.}$ equals a. Ahs reports that the near-equilibrium state can be reached relatively quickly (in several hours) by using a sample size of around 0.1 g. The extrapolation method was also used in this work [13] nevertheless.

2. Materials

A batch of cement pastes was prepared with a range of water to binder ratios from 0.33 to 0.50. As the aim of the work is to study the influence of high volumes of supplementary cementing materials applied in "ordinary" and high-performance concrete a polycarboxylate type superplasticizer (Glenium 51) was also applied in some cases. The use of superplasticizers is recommended for concrete designed for 28-d compressive strength above 30 MPa and/or slumps above 150 mm and containing supplementary cementing materials at the same time [14]. The use of pastes instead of concrete is founded on the basis of the literature search results, which show that the presence of the aggregates doesn't influence the water vapour sorption isotherms of the materials [10]. This can be explained by the fact that the micro- and meso-pores, where the moisture equilibrium processes described by the isotherms take place, are much smaller than the paste-aggregate interface inhomogeneities and the typical voids present in this zone. An overview of the samples' composition is given in Table 1. The chemical analysis of the materials used can be seen in Table 2.

The dry materials were mixed with water, cast into 40×40×160 mm moulds and then water cured for 28 days. After the water curing, the prisms were crushed and the fraction of the particles size between 0.5 and 1.0 mm was then placed into ~100% RH condition for approximately another 3 months. This particle size was chosen as the use of smaller particles can induce artefacts [10] and the use of coarser particles would prolong the time necessary to reach semi-equilibrium state.

Table 1
Sample composition (GBFS – granulated blast furnace slag, SP – superplasticizer).

Sample code	Sample composition [g]					W/B ratio	Sample age [months][a]
	CEM I 52.5 N	Silica fume	Class F fly ash	GBFS	SP		
C_33	100	–	–	–	–	0.33	4
C_40	100	–	–	–	–	0.40	4
C_50	100	–	–	–	–	0.50	4
CSP1_33	100	–	–	–	1	0.33	4
C90SF10_40	90	10	–	–	–	0.40	4
C50F50_40	50	–	50	–	–	0.40	4
C50F50SP1_33	50	–	50	–	1	0.33	4
C50S50SP1_33	50	–	–	50	1	0.33	4
C50S50_50	50	–	–	50	–	0.50	18
C15S85_50	15	–	–	85	–	0.50	18

[a] Values are indicating the age of the sample at the start of the experiments.

Carbonation and chemical aging are two different kinds of time-dependent processes that take place simultaneously during weathering. Both processes affect the pore structure and also the sorption behaviour. The age of the samples at the start of the water vapour sorption experiments was at least 4 months. At this age, the kinetics of ongoing hydraulic and pozzolanic reactions will be relatively slow. The effect of carbonation is further highlighted in the results section.

3. Experimental techniques

3.1. Water vapour sorption isotherms

For the determination of the water vapour sorption isotherms both semi-equilibrium (static) and dynamic methods were used. For the semi-equilibrium method the relative humidity environment was realised by means of keeping the samples in a desiccator above saturated salt solution or silica gel. The list of the salts used with the corresponding relative humidity values is shown in Table 3.

For the semi-equilibrium method, around 5 grams of the crushed and sieved sample was placed in a plastic dish, which was kept in the desiccator with the saturated salt solution. The desiccators were placed in a conditioned room at 20 °C. The sample was subsequently stored above the different salt solutions creating conditions of stepwise decreasing relative humidity to measure the desorption isotherm. Afterwards the adsorption isotherm was determined. The masses of the samples were logged periodically with an analytical balance (precision 0.0001 g), until no change above 0.001 g was observed during subsequent measurements after at least 24 h. The time necessary for

Table 2
Chemical composition of the materials used (mass-%) and specific surface (Blaine fineness in m^2/kg).

	CEM I 52.5 N	GBFS	Class F fly ash
CaO	63.12	40.38	2.47
SiO_2	18.73	34.35	49.34
Al_2O_3	4.94	11.36	24.55
Fe_2O_3	3.99	0.48	6.23
SO_3	3.07	1.65	0.30
MgO	1.02	7.57	1.73
K_2O	0.77	0.37	3.84
Na_2O	0.41	0.29	0.52
Cl^-	–	0.013	–
S^{2-}	–	0.77	–
Mn	–	0.165	–
Specific surface	390	400	330

Table 3
The saturated salt solutions used in the experiments and corresponding relative humidity at 20 °C [15].

Silica gel	LiCl	CH_3COOK	$MgCl_2$	NaBr	NaCl	KCl	$BaCl_2$	KNO_3	K_2SO_4
3%	12%	23%	33%	59%	76%	86%	90%	93%	97%

the development of an "equilibrium" state of the crushed samples was around two weeks. The mass water content of the samples at equilibrium condition is expressed as percentage of the sample mass in "dry" state. For this dry reference state, the equilibrium state reached at 3% RH after stepwise desorption was chosen. This avoids submitting the specimens to less mild and less controlled drying conditions, such as oven-drying, D-drying or freeze-drying.

For the water vapour sorption analysis by dynamic method (Dynamic Vapour Sorption, Surface Measurement Systems, London, UK), approximately 0.1 gram of dry sample (taken from the desiccator with silica gel, RH = 3%) was put on a dish placed in the chamber where the desired level of relative humidity was obtained by mixing a proportional amount of dry and humid nitrogen gas. The sample was vacuum dried and subjected to 0% RH in the dynamic vapour sorption equipment. The humidity value was then changed in steps of 10% each time the change of the sample mass in time was lower than 0.002 wt.% per minute till the target value of 90 or 95% RH was reached. Then the RH was decreased using the same value of the mass change in time as a criterium and a 10% RH step till the complete desorption curve was obtained. The equilibrium values were computed from the weight vs. time curves by extrapolation using the exponential function presented in Eq. (1). Examples of the typical humidity test cycle and the weight change response of the C_50 sample are shown in Fig. 1. Complete scanning of an adsorption and desorption curve using a RH step of 10% took approximately 48 h. Other researchers [11] have also used 1 min measuring intervals and a 24 h measuring time for the adsorption curve only of hardened cement paste.

3.2. Thermogravimetric analysis

The amount of chemically bound water and portlandite in samples was monitored by means of thermogravimetric analysis (TGA). At the age of testing, the specimens were crushed and soaked in methanol for one week to stop hydration completely. To avoid the influence of the methanol treatment, the specimens were stored in a dessicator over silica gel for another week [2,15]. The influence of methanol exchange is discussed more in detail by Baert et al. [2]. They found that replacement of the free water by methanol to stop the hydration had little or no effect on the measured amount of calcium hydroxide and chemically bound water in thermogravimetric experiments. However, the methanol replacement technique influenced to a limited extent the measured amount of calcium carbonate and led to a broader temperature range wherein calcium carbonate decomposed.

TGA was carried out from 20 °C to 1100 °C at rate of 10 °C per minute in argon atmosphere. The water chemically bound in the CSH is an integrated part of the structure of the gel solid and will mainly be driven off at temperatures above 105 °C. It was determined as the weight change of the sample between 105 °C and 1000 °C minus the loss on ignition of original components and minus the loss due to the decarbonation, which takes place around 670–700 °C [2]. The non-evaporable water content can be divided into two components, one due to the dehydration of calcium hydroxide around 450 °C and the other due to the dehydration of other hydrates. This separation can facilitate the study of pozzolanic and cementitious activity.

When CH decomposes (generally between 410 and 480 °C) in CaO and H_2O, a mass loss is recorded due to the loss of water. Taking into account the molecular weights of Portlandite (MW_{CH}) and water

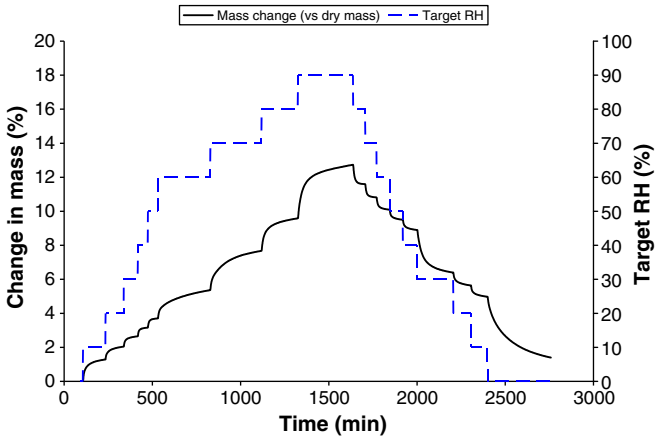

Fig. 1. Example of the humidity test cycle and the mass change response of the C_50 sample.

(MW_{H2O}), the weight loss in percent during CH dehydration (WL_{CH}) can be converted to the amount of CH according to Eq. (2).

$$CH(\%) = WL_{CH}(\%) \cdot \frac{MW_{CH}}{MW_{H_2O}} \tag{2}$$

Furthermore, the mass loss recorded at a temperature of ~670 °C corresponds with the decomposition of $CaCO_3$ in CaO and CO_2 (WL_{CaCO3}). Since the $CaCO_3$ originates on the one hand from the original components ($WL_{original\ CO2}$), but on the other hand from the chemical reaction between CH and CO_2 [16], an extra term is added to calculate the original CH content irrespective of carbonation, resulting in Eq. (3).

$$CH(\%) = WL_{CH}(\%) \cdot \frac{MW_{CH}}{MW_{H_2O}} + \left(WL_{CaCO_3}(\%) - WL_{originalCO_2}(\%)\right) \cdot \frac{MW_{CH}}{MW_{CO_2}} \tag{3}$$

Moreover, the mass losses WL_{CH} and WL_{CaCO3} were corrected for the concurrent dehydration of all other hydrates, according to the method described by Baert [2,15].

3.3. BET method specific surface calculation

Nitrogen sorption isotherm experiments were carried out at 77 K temperature. The cement paste samples were dried at 105 °C and degassed before the experiments. Like in case of water vapour sorption isotherms, the nitrogen adsorption isotherms strongly depend on the way of sample preparation. It has been shown by comparison of BET_{N2} results of the same sample, that the obtained specific surface values depend on the means of sample preparation in the following order: methanol exchange + D-drying > D-drying > oven drying (105 °C) [17].

4. Results and discussion

4.1. Thermogravimetric analysis

The results of thermogravimetric analysis are summarized in Fig. 2 and Table 4.

The thermogravimetric analysis results show an increasing amount of portlandite (calculated according to Eq. (3), including carbonated portlandite) in pure portland cement pastes samples with increasing water to cement ratio. As expected, the amount of the portlandite in the sample is lower when latent hydraulic or pozzolanic

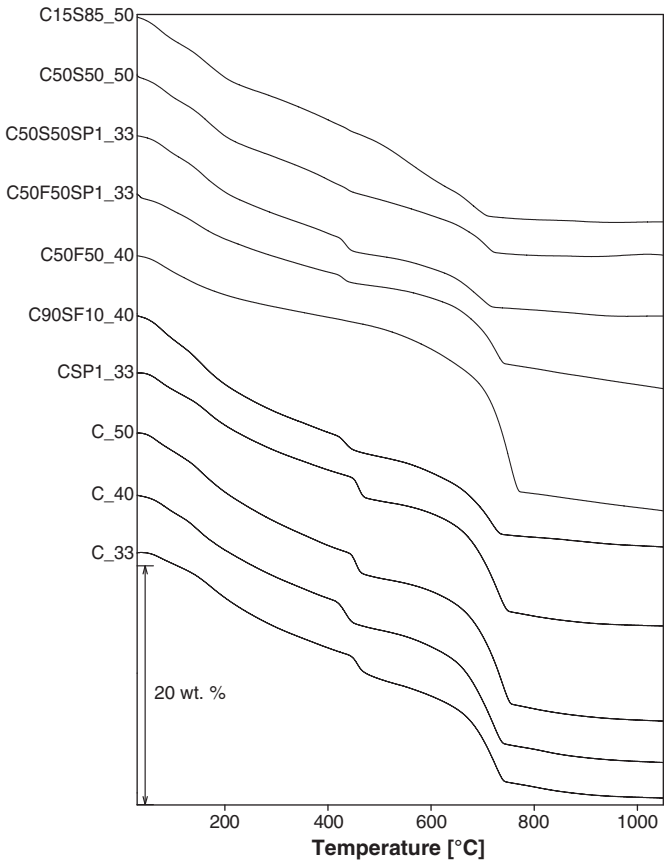

Fig. 2. TGA analysis of the samples.

active constituents are used. This is most pronounced in case of use of GBFS in older (1.5 years) samples and in samples containing fly ash.

At the time of measurement, all samples were partially carbonated. Even though carbonation is generally supposed to be negligible for high RH values, due to an almost impossible CO_2 diffusion through the gaseous porous network, carbonation may occur here in aqueous phase by the direct action of carbonate/bicarbonate ions migrating within the pore solution after dissolution. Though this aqueous carbonation takes longer time than atmospheric carbonation, it is reasonable to observe a high level of carbonation on crushed samples after a 3-month curing period. For most samples 60 to 70% of the portlandite was carbonated. The carbonation process had even further progressed in the sample containing 50% of fly ash (C50F50_40) (93% of the portlandite carbonated). However the similar sample containing superplasticizer and having lower water to binder ratio (C50F50SP1_33) is showing only a moderate level of carbonation — this can be due to the denser microstructure formed when superplasticizer and lower water to cement ratio is used. This effect is most apparent from the comparison of the results of BET_{N2} adsorption specific surface measurement of C50F50_40 (33 m^2g^{-1}) and C50F50SP1_33 (20 m^2g^{-1}) samples (see further). These results indicate that samples having lower water to cement ratio, have less surface available to nitrogen molecules and also water molecules. Also the sample C50S50_50 showed a more elevated carbonation degree (80%), due to the lower amount of portlandite in cement paste with blast furnace slag and at later ages (5.8% total portlandite content). For the sample C15S85_50, in which 85% of the binder consisted of slag, the total portlandite content (in original and in carbonated form) was extremely low (1.1%).

Table 4
Results of thermogravimetric analysis of the samples.

Sample code	Thermogravimetric analysis results [wt.%]	
	Portlandite content	Chemically bound water
C_33	17.4	11.0
C_40	19.7	11.0
C_50	22.4	11.4
CSP1_33	20.3	10.0
C90SF10_40	12.5	10.3
C50F50_40	16.5	6.9
C50F50SP1_33	7.5	7.9
C50S50SP1_33	9.5	8.8
C50S50_50 (age 1.5 years)	5.8	8.7
C15S85_50 (age 1.5 years)	1.1	10.5

Carbonation is a natural process which will also occur in realistic situations for the outer concrete layer (which is the most important one with regard to degradation processes). Therefore it is important to investigate the pore size distribution particularly for carbonated concrete. The samples which are most carbonated are those with a high volume of fly ash or slag. This is also noticed in real structures for concrete elements with such binder composition. Further carbonation during the measurements itself is negligible, as is also mentioned by other researchers [10,18]. As a consequence of carbonation, porosity may be reduced (case of CEM I) or increased (when the content of fly ash, slag or silica fume is high). In the case one wants to prevent carbonation, the samples should be stored under vacuum or low gas pressure before and during the measurements. Alternatively, soda lime could be used to avoid carbonation.

4.2. Static water vapour sorption isotherms

The water vapour sorption isotherms of the samples obtained by the semi-equilibrium method are shown in Fig. 3(a) for the samples with ordinary Portland cement or with silica fume addition, and in Fig. 3(b) for the samples with fly ash or slag.

The results exhibit hysteresis between desorption and adsorption curve over the whole range of relative humidity. For the samples with fly ash, the hysteresis is most limited. The water uptake of samples without additions is of the same order of magnitude as described in literature for similar samples, e.g. the adsorption and desorption curves measured with the static semi-equilibrium method by Baroghel–Bouny [10] for hardened cement paste with $w/c = 0.45$, fit nicely between our adsorption, respectively desorption curves of C_40 and C_50. Water-to-cement ratio and overall mix composition have a clear influence on the desorption isotherms, while the effect on adsorption is much more limited. Although at desorption differences in water content between mixes become more pronounced from a RH of 33% onwards, an effect of mix composition can already be noticed for RH as low as 12%. In work of Baroghel–Bouny [10] the desorption isotherms were, on the contrary, identical for different mixes at RH<44%. However, normalisation of our desorption isotherms by the CSH content, reduces the differences for RH<44%.

4.3. Pore size distribution

The pore size was determined using the Barett, Jonyer and Halenda (BJH) method [19], which allows the determination of the pore size distribution in mesopore range from the desorption part of the isotherm. The basic assumption of this method is the coexistence of capillary and adsorbed water phases in cylindrical pores. In spite of the differences between the cylindrical pore model and actual cement paste microstructure, the BJH calculation can provide information useful at least for comparative studies. The method makes use of the Kelvin Eq. (4), which relates the equilibrium vapour pressure of a curved surface, such as that of a

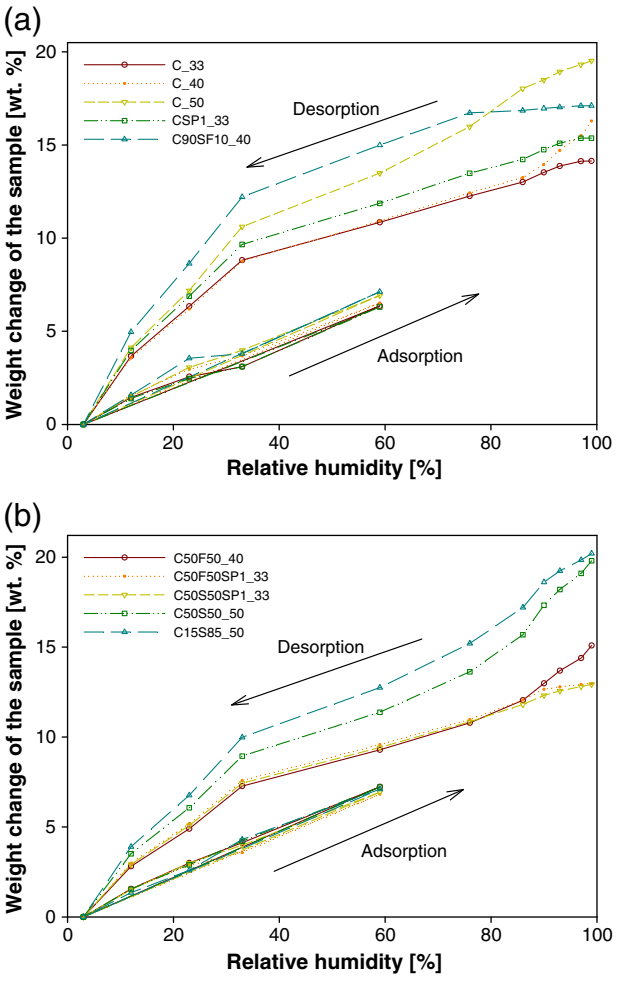

Fig. 3. Results of semi-equilibrium water vapour sorption analysis for (a) the samples with ordinary Portland cement or with silica fume addition; (b) the samples with fly ash or slag.

liquid in a capillary or pore to the equilibrium pressure of the same liquid on a plane surface:

$$\ln\frac{p}{p_0} = -\frac{2\gamma\,\overline{V}}{r_k RT}\cos\theta \tag{4}$$

where p is the equilibrium vapour pressure of the liquid contained in a pore of radius r_k (Kelvin radius) and p_0 is an equilibrium pressure of the same liquid at a plane surface. The γ is liquid surface tension, $\overline{V}$ is the molar volume of liquid, θ is the contact angle between the liquid and the pore wall, R is the universal gas constant ($8.314\,\mathrm{J\,K^{-1}\,mol^{-1}}$) and T is the thermodynamic temperature. For the water vapour sorption on the polar surface of the cement paste pores the following applies: $\gamma = 7.28\times10^{-2}\,\mathrm{N\,m^{-1}}$, $\theta = 0$ and $\overline{V} = 17.98\times10^{-3}\,\mathrm{l\,mol^{-1}}$.

However the Kelvin radius is not the actual pore radius, because some adsorption has occurred on the pore wall prior to condensation, or, in case of desorption, a film of adsorbed water will remain on the pore wall after the evaporation of the pore core. The actual pore radius r_p is thus sum of the Kelvin radius r_k and thickness t of adsorbed film at given relative humidity (p/p_0). The relation between adsorbed film thickness and relative humidity used in BJH calculations in this article (t-curve) for adsorption of the water vapour on the non-porous surface with the heat of adsorption similar to the heat of adsorption of the studied materials was determined by Hagymassy et al. [20] as cited by [10] (see Fig. 4). The procedure of BJH calculation, which was applied on the data is described in [19].

Pore size distribution of pure portland cement samples and a sample containing 10% by weight of silica fume (Fig. 5(a)) and of samples containing additions (Fig. 5(b)) exhibit significant differences. Generally, the pure portland cement samples with w/c-ratio of 0.3 or 0.4 show a finer pore network with more micropores (<2 nm) and less mesopores. The effect of water-to-cement ratio is apparent, mainly on the C_50 sample (w/c ratio 0.5), which exhibits a second maximum on the pore size distribution curve around pore radius of approximately 6 nm. This sample has less micropores a larger amount of capillary pores.

The samples with additions and similar water-to-binder ratios as pure Portland cement samples, have of course a higher water-to-cement ratio. Still, the mixes with FA or GBFS and water/binder ratio of 0.33 or 0.40 have a similar pore size distribution above 2 nm (pore radius) as the pure Portland cement pastes with the same water/binder ratio. The high amount of 1 nm radius pores that is present in the Portland cement pastes is lacking, however, in the pastes with FA and GBFS. This is not so for the paste with SF, which shows a high amount of micropores (radius around 1 nm) and also the highest amount of gel pores in the mesopore range (radius 1 to 5 nm), which is in line with the higher amount of CSH gel in this mix (see further).

The pastes containing GBFS at older age (1.5 yr) show less capillary pores than the pure cement paste with the same water/binder ratio (C_50) at 4 months of age. The course of their pore size distribution is far more "flat" and this observation was most pronounced for the sample containing 85% of GBFS (C15S85_50).

In [10] the isotherms are partitioned in relevant RH ranges, where equilibrium water contents are more or less affected by mix parameters:

- For RH>76% there is a prominent influence of W/C; this RH-range corresponds to the pure capillary porosity range, with pore radii>5 nm according to BJH calculations. This W/C effect is also clear in the current results: there is a clear increase in water content for C_40 and C_50, compared to C_33 above 76% RH (Fig. 3(a)). Also, C50F50_40 starts to deviate clearly from C50F50SP1_33 in this RH range, and C50S50_50 differs increasingly from C50S50SP1_33 (Fig. 3(b)).
- For RH between 50–76% (corresponding to "gel" pore radii between 2 and 5 nm) the effect of W/C is reduced and also other mix parameters have their influence. In this range water is removed by desorption between outer (low density) CSH products. The desorption isotherms of the tested mixtures have all reasonably low and relatively similar slopes in this range, only for the mixes with the highest W/B ratio (0.50) the slope is somewhat larger, indicating that these mixes have a larger volume of 2–5 nm pores.
- For RH<50%, corresponding to BJH pore radii below 2 nm, the effect of the mix composition can be attributed to different CSH amounts. It may be a point of discussion whether differences may also be attributed to a more refined gel pore structure. However, Jennings [21] indicates that the specific volume of gel pores is experimentally nearly constant (as well as the specific surface area measured by water), since the small gel pores are roughly the same size. The highest values here are obtained for the mix with SF addition and also reasonably high values are noticed for the mixes with high W/B (0.5). For C50S50_50 and C15S85_50 also the longer curing period will have an effect.

4.4. Dynamic water vapour sorption isotherms

An example of a water vapour sorption isotherm obtained by the dynamic method is shown in Fig. 6. There is a clear divergence between the first and subsequent adsorption curves, while after the first adsorption process, the following adsorption, respectively desorption isotherms overlay each other. This irreversibility in mass in the dry state was not noticed in the static experiments and can be ascribed to the stronger drying method (vacuum drying) in the case of the dynamic tests. This drying technique seems to remove interlayer water from the

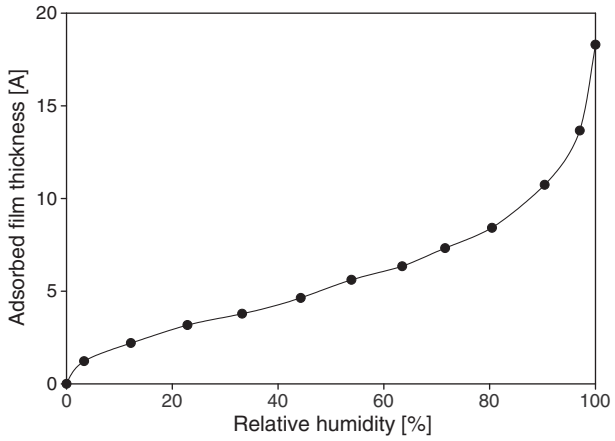

Fig. 4. *t*-curve published by Hagymassy for non-porous adsorbents with similar heat of adsorption as the materials studied [20] as cited by [10].

CSH, which re-enters when RH increases again. Less severe drying during subsequent RH-cycling in the dynamic vapour sorption equipment, does not remove this interlayer water again. This can be interpreted in light of literature on different types of water in CSH [22,23]. This shows that the chemical formula of CSH is actually $C_{1.7}SH_{1.8}$, including evaporable and non-evaporable water within the saturated CSH particles, but not surface adsorbed water. Of this 1.8 mol water, 1.3 mol is chemically bound (and thus maintained in d-dried state); and 0.5 mol is the interlayer space in which tiny gel pores are entrapped (called intraglobular pores, with size below 0.5 nm, in [21,23]). Additionally, 0.3 mol water forms an outer monolayer at relative humidity above 11%, which would lead to the formula of $C_{1.7}SH_{2.1}$ when this adsorbed surface water is included. During desorption to 0% RH, the monolayer water (0.3 mol) and part of the interlayer water (0.25 mol) is removed. Only when more severe drying techniques are applied, the remaining interlayer water is removed and collapse of the sheet like CSH structure occurs. This water will only reenter at higher RH, probably above 60%, where the first and subsequent adsorption curves in Fig. 6 no longer run parallel. Since removal of this strongly bound interlayer water appears to be reversible (although only at higher RH, so that some authors call it "irreversible"), we consider that it does not enhance chemical ageing as is described by other authors [10,24].

For the samples under discussion in the current study, the difference in mass water content in the dry state, due to the removal of strongly bound interlayer water through vacuum drying as explained above, amounts to $1.99 \pm 0.34\%$ at around 0% RH for the 4 month old samples, and $0.16 \pm 0.08\%$ for the 1.5 year old samples, which could be explained by a more firm binding of the interlayer water in the CSH at later age. This can be related to the chemical ageing effect, increasing the degree of polymerisation of the CSH silicate chains and changing them in stronger and denser ones [10]. Furthermore, enhanced carbonation at later ages (1.5 year vs. 4 months, see Section 4.1), which decomposes part of the CSH to vaterite or calcite and silica gel, may have reduced the amount of interlayer water.

In Fig. 7 the desorption and adsorption isotherms are shown for the different pastes, leaving out the deviating first adsorption curve, and with correction for the removed interlayer water. From the dynamic water vapour sorption isotherms, some similar conclusions can be drawn as for the static experiments. Again the effect of the water-to-cement ratio is clear, with higher ratios giving higher mass water contents at the same RH. Silica fume increases the amount of gel pores with pore radii below 2 nm. Again, for the samples with fly ash, the hysteresis is most limited.

However, the absolute values for mass water content are on average 1.7 times lower in dynamic vs. static experiments. Different explanations are possible. In the dynamic experiments, no measurements were taken above 90% RH, whereas in the static experiments the samples were submitted to humidities up to 97%. As can be seen also in work of other researchers [10,18] the mass water content in the paste is increasing significantly between 90 and 97% RH. Espinosa et al. [18] found that desorption curves starting from different RH run parallel. Therefore, the desorption isotherms are located at quite a bit higher water contents if their initial RH is higher. Tada and Watanabe [11], however, measured with the dynamic method very similar adsorption isotherms for Portland cement pastes with *w*/*c* equal to 0.3, 0.4, and 0.5 as the adsorption curves for similar pastes in the current research. Nevertheless they also tested up to RH values of 95%. Their values were on average 1–2% higher than ours, but they only measured the first adsorption isotherm after drying in dry air of a dew point temperature of –42 °C. This is milder than the D-drying method (dry air at dew point temperature of −76 °C), but more severe than conditioning at 0% RH in the dynamic vapour sorption apparatus. Hence, the re-entry of CSH-interlayer water is included in their curves. As mentioned above, this effect reduced the mass water contents measured in our experiments from the second desorption onwards, by about 2%. Correcting for the re-entry of firmly bound interlayer water, would therefore provide an excellent correspondence between the results of Tada and Watanabe [11] and ours. Furthermore, they claim to see a good correspondence between their dynamic measurements on cement paste with *w*/*c* of 0.3 and the adsorption isotherm determined by Yuasa [25] using saturated salt solutions [11].

Since from the former it may be concluded that the results of the dynamic experiments are correct, the reason for the differences between our static and dynamic isotherms may be found in the different conditioning before testing. Samples for static experiments were cured and conditioned at 100% RH, after which the first desorption isotherm was determined. For the dynamic experiments, actually the first desorption isotherm is lacking, since samples were taken from the 3% RH dessicator and then vacuum dried. To investigate the effect of the different conditioning method, a sample with similar composition as C_50, was brought in the dynamic vapour sorption equipment in saturated conditions and then equilibrated at 100% RH. The procedure is therefore much more similar to the one during the static experiments and indeed so is the first desorption isotherm shown in Fig. 8.

Furthermore, it can be noticed in Fig. 8 that the high mass water contents at the start of the first desorption is not reached again during subsequent RH cycles and large deviations between first and subsequent desorption isotherms are seen especially above 50% RH. Different literature sources describe an instability of the pore structure during the first desorption [10]. Jennings states that drying below 40% RH causes irreversible collapse of low density CSH [24,26] and thus changes the CSH in stiffer, stronger and denser ones. The pore structure is considered more stable after this first desorption. Since the drying is thought to enhance chemical ageing and increase the degree of polymerisation of the silicate chains, the curves starting from the second desorption are supposed to be more representative of the pore structure. Other authors such as Ahs [13] stopped desorption at 10% RH to avoid the risk of damage to the pore structure. To check if the pore structure would change by subjecting the cement paste to low relative humidity (and if this would be the reason for the difference between first and second desorption), for the experiment shown in Fig. 8 the first desorption was limited to a RH of 10%. Nevertheless, still the difference at medium to high RH between first and second desorption curves was noticed, and this difference did not increase (at the end of the second adsorption) when the RH was further decreased to 0% in the second desorption curve. A similar observation was made when the first desorption was restricted to 30% RH (Fig. 9). Also, although we did not measure more than one desorption isotherm in the static experiments, literature data show that with the semi-equilibrium method using saturated salt solutions,

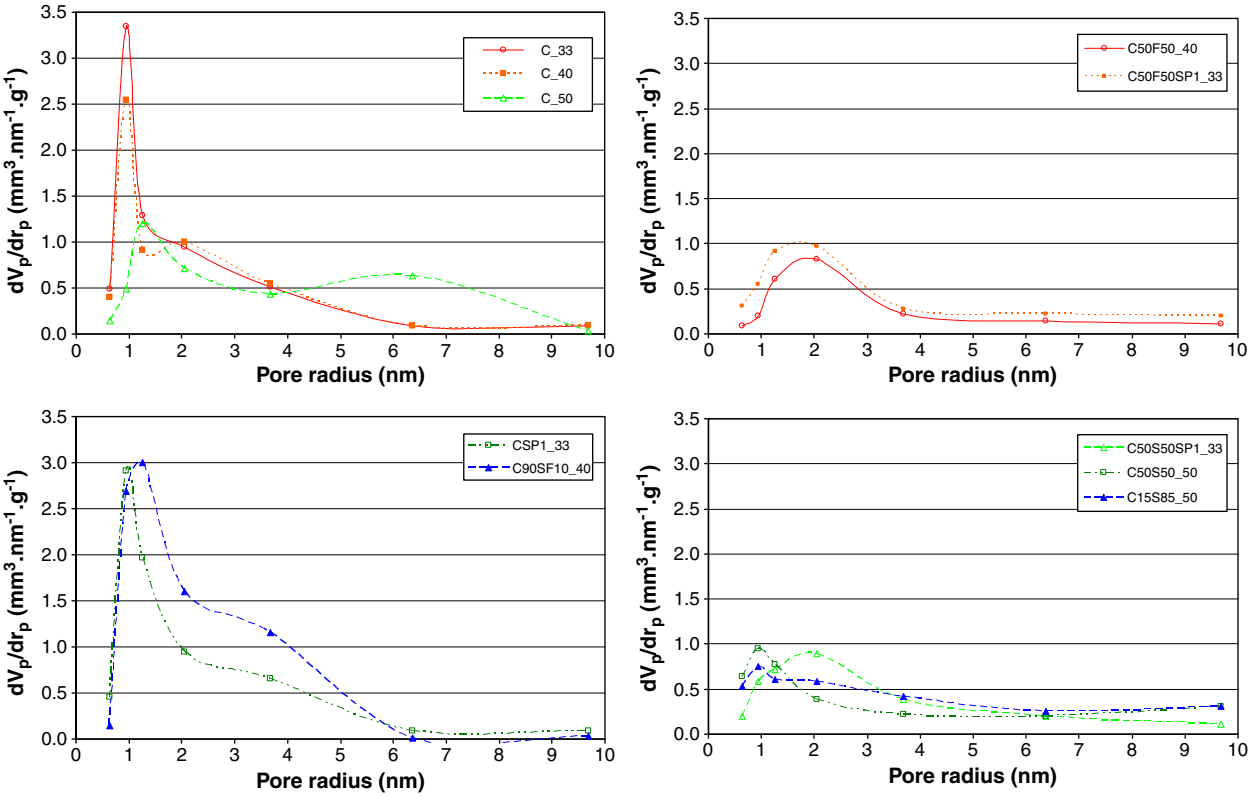

Fig. 5. Pore size distributions calculated from water vapour sorption isotherms (BJH calculations).

second and third desorption isotherms from 100% RH overlay the first one [10]. From the above it can be concluded that the difference between first and subsequent desorption curves for our samples is not caused by a change in pore structure due to chemical ageing. When the experiment in Fig. 9 was carried out a second time (one month later) on the same sample, after water saturation and equilibration at 100% RH, the dynamic sorption experiment yielded quite similar isotherms (Fig. 10) as before. This proves that the difference between first and subsequent desorption curves is mainly caused by a more full saturation of macropores at the start of the experiment, than can be reached in the DVS equipment by increasing the RH after drying at low RH.

The only remaining question is now, why more full saturation of the pore system can be reached in static compared to dynamic experiments. We hypothesise that the choice of the procedure affects the transition point from hygroscopic into over-hygroscopic water content. This point is difficult to define and varies according to literature between 94% and 99% RH [18]. Below this transition water content, adsorption and capillary condensation set in micro- and mesopores, whereas above 95% RH, condensation is presumed in macropores (>50 nm). The results appear to indicate that macropore condensation is only taking place in the static, and not in the dynamic vapour sorption tests, resulting in a more full saturation of the pore structure. This can easily result in differences in mass water content at 100% RH of more than 10%.

Since hysteresis loops of this type do not close until the equilibrium RH is very close to saturation, the location of the desorption branch depends very much on the real maximum RH attained before commencement of desorption. It is therefore advisable to start desorption from a completely saturated substrate (bulk condensation, submersion in water), in order to determine the true boundary desorption isotherm and hence the extent of the hysteresis loop [27].

Another difference between the sorption isotherms measured in dynamic or static experiments, is that in the dynamic tests there is a larger difference to be noticed between the adsorption curves, depending on the mix composition.

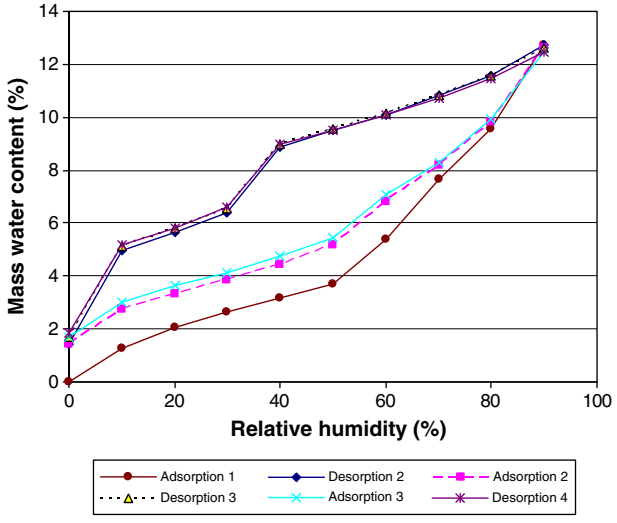

Fig. 6. Dynamic water vapour sorption isotherms for sample C_50.

4.5. BET method specific surface calculation

For determination of the specific surface of hydrated cements the nitrogen adsorption and water vapour adsorption techniques were used and the results were compared. The calculation of specific surface is based on the BET method, which is a widely used and established approach of determining the specific surface area of solid

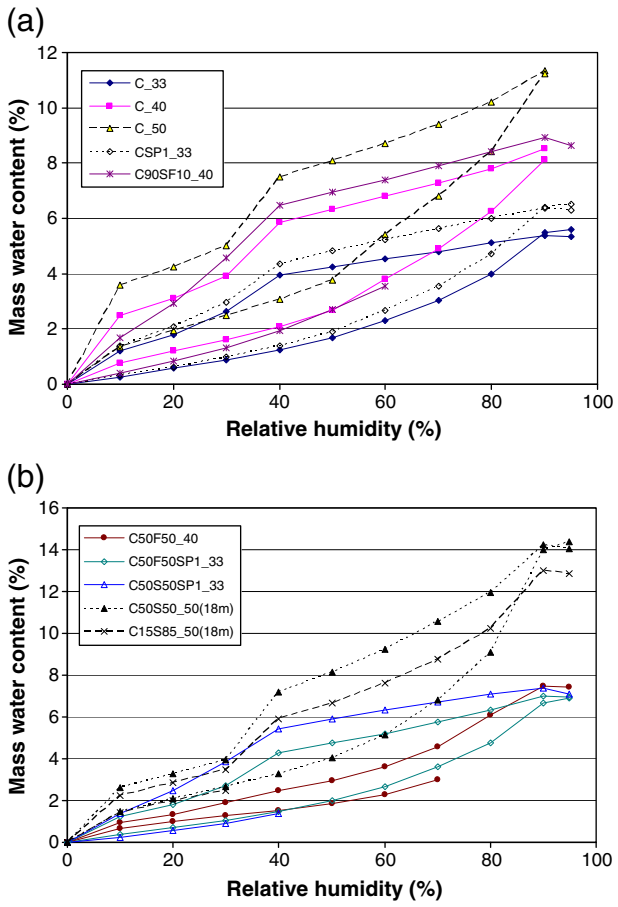

Fig. 7. Desorption and adsorption isotherms for the different pastes, corrected for re-entry of CSH interlayer water, for (a) the samples with ordinary Portland cement or with silica fume addition; (b) the samples with fly ash or slag.

materials, especially such with distinct open porosity, using Eq. (5) suggested by Brunauer et al. [28].

$$\frac{p}{v\cdot(p_0-p)} = \frac{1}{v_m\cdot C} + \frac{(C-1)}{v_m\cdot C}\cdot\frac{p}{p_0} \tag{5}$$

where v is a volume of the adsorbed substance (water or nitrogen) and p and p_0 are equilibrium pressure and saturation pressure on a free surface (which in case of the water vapour can be substituted by

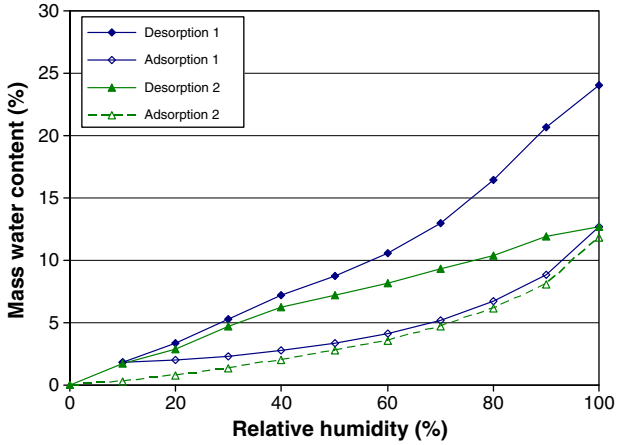

Fig. 8. Dynamic water vapour sorption isotherm for a sample similar to C_50, with the first desorption starting from saturated conditions and restricted to 10% RH.

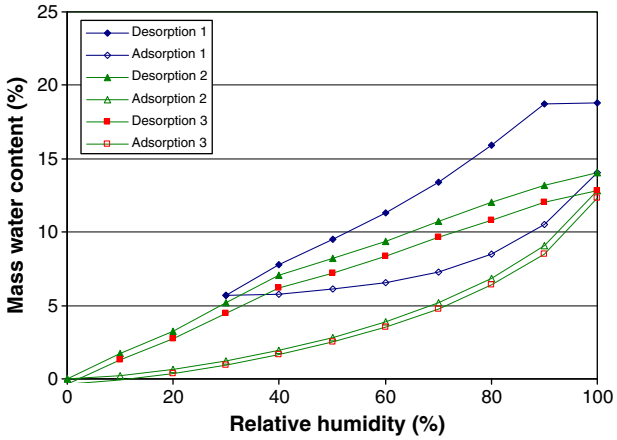

Fig. 9. Dynamic water vapour sorption isotherm for a sample similar to C_50, with the first desorption starting from saturated conditions and restricted to 30% RH.

RH values in %); v_m is the volume of the adsorbent which is adsorbed on the sample in case of monolayer adsorption and C is a constant which characterises the interaction between sample and adsorbed gas (a large value of C indicates a large interaction).

For purpose of this calculation the experimental data in the low pressure region (p/p_0 of 0 to 0.30) were plotted as a straight line $p/[v\cdot(p_0-p)]$ vs. p/p_0. This line intersects the Y-axis in $I=1/(v_m\cdot C)$ and has a slope $A=(C-1)/(v_m\cdot C)$. The volume of the adsorbent in case of monolayer adsorption v_m can then be calculated using Eq. (6):

$$v_m = \frac{1}{A+I} \tag{6}$$

The specific surface S_{BET} was then calculated from the known area occupied by one molecule of the adsorbed substance (for the calculations in this study the value s_m of surface area of 0.114 nm^2 for the molecule of water and 0.162 nm^2 for the molecule of nitrogen [7]) using Eq. (7):

$$S_{BET} = \frac{v_m\cdot N_A\cdot s_m}{V} \tag{7}$$

where N_A is Avogadro's number, V is molar volume. The specific surface results from various methods are presented in Table 5.

The specific surface values obtained by means of BET_{H2O} method and BET_{N2} method show big differences. This observation was also made by other authors; however different interpretation of this phenomenon is given in literature. One possible explanation is that the higher values of specific surface results of the BET_{H2O} method are

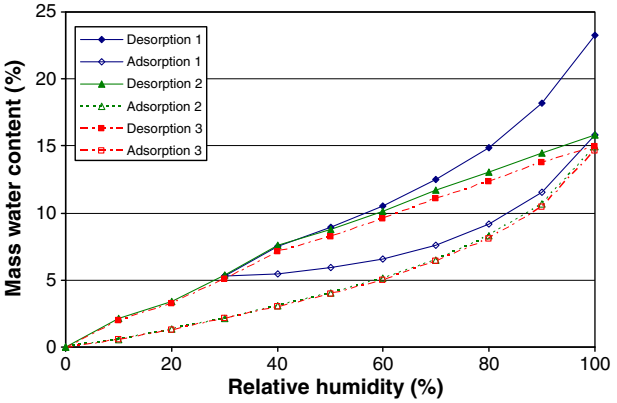

Fig. 10. Dynamic water vapour sorption isotherm for the same sample as in Fig. 8, one month later and after resaturation.

observed because a fraction of the water molecules enters the space between CSH layers, from where the originally bound water was removed during sample preparation, which leads to erroneously high BET_{H2O} results. According to another view, bigger nitrogen molecules are not able to penetrate the whole existing pore space, thus obtained BET_{N2} values indicate only the specific surface which is located in pores accessible to this adsorbate. However, the pores not filled with N_2, have an average diameter several times exceeding the diameter of the nitrogen molecule. Odler [7] has shown that the lower BET_{N2} results are mainly due to the low temperature and too short equilibration time employed in the case of N_2 adsorption. Due to differences in the vaporization characteristics of nitrogen and water, the adsorption data needed for BET_{N2} and BET_{H2O} determinations have to be collected at different temperatures, typically at the boiling temperature of liquid nitrogen (77 K) for BET_{N2} and at ambient temperature for BET_{H2O}. Penetration of the adsorbate molecules into spaces accessible only through very narrow openings (called ink bottle pores) can take place only by activated diffusion, the rate of which — unlike that of normal diffusion — is highly temperature dependent. It was estimated that because of differences in the employed temperature of adsorption, water should pass over the energy barrier about 50 times more rapidly; thus, it would take nitrogen several years to equilibrate. All these facts indicate that BET_{N2} values do not represent the total surface area of C–S–H-based materials and the BET_{H2O} values appear to be more correct in this respect [7].

Fig. 11(a) and (b) shows the correlations of $BET_{H2O(static)}$ specific surface area and BET_{N2} specific surface area with water to binder ratio. The BET_{H2O} is mostly influenced by the specific surface area of CSH. Apart from it, hydrated portland cement pastes contain portlandite (which's specific surface area is negligible [7]) and usually small amounts of ettringite ($C_6AS_3H_{32}$) and/or monosulfate (C_4ASH_{12}). The latter two phases would decompose under D-drying conditions but the contribution to the weight gain of the sample at low relative water vapour pressures used in BET_{H2O} determination is also negligible [7].

Generally, linear correlations were found in both cases; however there are some interesting deviations between the results obtained by BET_{H2O} and BET_{N2} methods, which were observed in case of the samples containing 10% of silica fume (C90SF10_40) and pure portland cement sample with superplasticizer (CSP1_33). The most pronounced is the difference of the results obtained for the C90SF10_40 sample — in case of the BET_{H2O}, the value of specific surface is significantly above the observed linear trend. The cause of this effect, observed also by other researchers [10], is probably the higher amount of CSH gel generated from pozzolanic reaction between portlandite and silica fume particles, as silica fume is highly pozzolanic active. On the other hand, the results obtained by using the BET_{N2} method on the same sample are slightly below the observed linear trend. It is clear that an introduction of silica fume into the sample results in an increase of specific surface (especially by increasing the amount of pores<5 nm, cf. Fig. 5(a)), which is not accessible to nitrogen molecules. In case of the CSP1_33 sample, an opposite phenomenon was observed. Possible explanation for this observation is, that due to the dispersion effect of superplasticizer, more accessible micropore structure of the hydrated cement paste for nitrogen molecules is created. However, further research to prove this assumption is required, as the same effect of superplasticizer was not observed in case of samples containing mineral admixtures (C50S50SP1_33 and C50F50SP1_33).

Table 5
Specific surface of the samples studied.

Sample code	Specific surface results [m^2g^{-1}]		
	BET_{H2O} static	BET_{H2O} dynamic	BET_{N2}
C_33	110	78	12
C_40	113	82	15
C_50	123	101	24
CSP1_33	111	96	25
C90SF10_40	124	114	16
C50F50_40	130	108	33
C50F50SP1_33	119	103	20
C50S50SP1_33	124	109	20
C50S50_50 (age 1.5 years)	131	118	41
C15S85_50 (age 1.5 years)	135	121	67

4.6. CSH "gel" amount determination

The quantity of C–S–H in hydrated portland cement samples can be determined using indirect techniques, such as loss on ignition or quantitative X-ray determination of unreacted cement and calcium hydroxide. It is however difficult to measure CSH content directly due to both a lack of crystallinity and not precisely defined composition. The direct method for quantification of CSH gel content based on the water vapour sorption technique was developed by Olson and Jennings [29]. Principle of the technique lies in the fact, that CSH gel has a surface area per unit volume at least an order of magnitude higher than any other component in hardened Portland cement paste [7,29]. If a unit mass of dried CSH adsorbs a specific amount of water when equilibrated at a specific RH and all dried CSH is equally accessible to water, then the quantity of CSH in a cement paste can be deduced. For the determination of CSH content, the RH value between 11% and 50% is most suitable, as below 11% the mass uptake vs. RH is not linear because less than the equivalent of a full monolayer is present and also not linear above 50% RH because of the starting of condensation of the water in pores [29]. In this study the RH value of 23% was chosen — the sample, previously dried in 3% RH environment, was placed into a desiccator with CH_3COOK saturated solution. The weight gain of 1 cm^3 of CSH gel under these conditions as determined by Baroghel–Bouny [10] is 0.219 g. The results of CSH gel amount determination by aforementioned method are shown on Fig. 12.

The results obtained show that the higher the water-to-cement ratio, the higher the CSH gel content. The highest CSH gel content was measured for sample C90SF10_40 (containing 10% of silica fume). This can be explained by additional CSH gel formation by the pozzolanic reaction of silica fume with portlandite. The CSH content measured in other samples containing supplementary cementing materials were relatively similar and in some cases surprisingly high, when compared to the samples containing pure portland cement, as the content of portland cement in these samples was 50 or even 15 wt.% respectively. This can be explained by additional formation of CSH due to the pozzolanic reaction of secondary cementitious materials since the samples were tested at the ages of 4 and 18 months, and also by the higher amount of water available for portland cement hydration.

5. Conclusion

The work presented in this paper summarises the results of an application of water and nitrogen adsorption experiments to study the microstructure of cement pastes and the influence of secondary cementitious materials (class F fly ash, granulated blast furnace slag and silica fume).

The results exhibit hysteresis between water vapour desorption and adsorption curves over the whole range of relative humidity. For the samples with fly ash, the hysteresis is most limited. Water-to-cement ratio and overall mix composition have a clear influence on the desorption isotherms for RHs of 12% and more, while the effect on adsorption isotherms obtained with the static method is limited.

Calculation of the pore size distribution of the samples using the BJH method starting from the water vapour desorption curves in the micro- and mesoporous range, allows to estimate the effects of mix composition. An increased amount of capillary pores is obtained with higher water-to-cement ratio (0.5 vs. 0.3 and 0.4). Replacement of

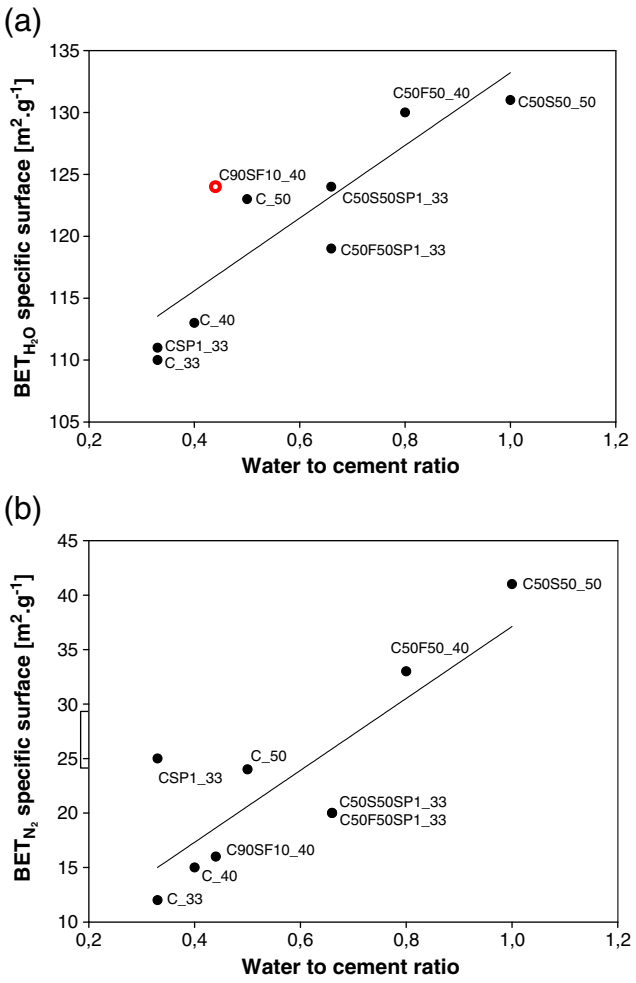

Fig. 11. (a): Correlation between BET_{H2O} specific surface area and water to cement ratio. (b): Correlation between BET_{N2} specific surface area and water to cement ratio.

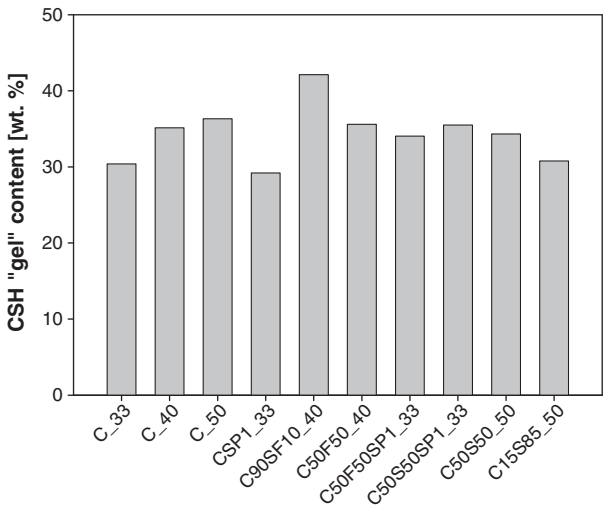

Fig. 12. CSH gel content determined from water vapour sorption analysis.

50% or more of the Portland cement with fly ash or slag, mainly decreases the amount of micropores (pore width<2 nm). This is not so for the paste with SF, which shows a high amount of micropores and also the highest amount of gel pores in the mesopore range (pore width 2 to 10 nm). This is in line with the higher amount of CSH gel in this mix, calculated based on the water vapour adsorption values at 23% RH. Pastes containing GBFS at older age (1.5 yr) show less capillary pores than pure cement paste with the same water/binder ratio (0.5) at 4 months of age.

Regarding the comparison of the static water vapour sorption method, dynamic water vapour sorption method and nitrogen sorption method applied on the cement pastes, the following observations were made:

- The predrying method influences the sorption isotherms. Vacuum drying removes firmly bound interlayer water from the CSH in a reversible way, without enhancing chemical ageing. This water will only re-enter at high relative humidity (probably above 60%). The magnitude of this effect decreases with sample age.
- The results appear to indicate that full macropore condensation is only taking place in the static, and not in the dynamic vapour sorption tests, resulting in a more full saturation of the pore structure in the former. This can easily result in differences in mass water content around 100% RH of more than 10%. Since the hysteresis loops do not close until the equilibrium RH is very close to saturation, the location of the desorption branch depends very much on the real maximum RH attained before commencement of desorption. It is therefore advisable to start desorption from a completely saturated substrate (bulk condensation, submersion in water), in order to determine the true boundary desorption isotherm and hence the extent of the hysteresis loop.
- Specific surface computed by BET method from $BET_{H2Ostatic}$ and $BET_{H2Odynamic}$ is comparable, the differences can be accounted for by the sample preparation history as for the dynamic water vapour sorption the samples were vacuum dried before the experiment.
- The BET_{N2} specific surface is considerably lower for all the samples. There are several possible explanations for this phenomenon. With water vapour sorption, upon adsorption a fraction of water molecules enters the space between CSH layers, from where the originally bound water was removed during sample preparation, which leads to erroneously high BET_{H2O} results. According to another view, nitrogen molecules are not able to penetrate the whole existing pore space at the low temperatures applied in these experiments, thus obtained BET_{N2} values indicate only the specific surface which is located in pores accessible to this adsorbate. Some influence can also be accounted to the different sample preparation procedure (drying at 105 °C and degassing).

For the characterisation of the samples, thermogravimetric analysis was also used, showing the influence of the water to cement ratio and mainly of the presence of the pozzolanic active materials on the portlandite content in the sample and also on the level of carbonation of the sample. A linear relation was observed between specific surface measured by both methods and water to cement ratio of the samples. In case of introduction of silica fume into the sample, an increase of specific surface is noticed, which is accessible to water, but not to nitrogen molecules.

Acknowledgments

The authors wish to acknowledge the Research Foundation Flanders (FWO-Vlaanderen, project B.0.135.05) and the Ghent University Research Fund (BOF-UGent, project 01115005) for the financial support.

References

[1] P.-C. Aïtcin, High Performance Concrete, Taylor & Francis, 1998.
[2] G. Baert, S. Hoste, G. De Schutter, N. De Belie, Reactivity of fly ash in cement paste studied by means of thermogravimetry and isothermal calorimetry, Journal of Thermal Analysis and Calorimetry 94 (2) (2008) 485–492.
[3] K.A. Kalliopi, Pore Structure of Cement-based Materials: Testing, Interpretation and Requirements, Taylor & Francis, 2006.

[4] A. Wang, C. Zhang, W. Sun, Fly ash effects: I. The morphological effect of fly ash, Cement and Concrete Research 33 (12) (2003) 2023–2029.
[5] G. Li, X. Zhao, Properties of concrete incorporating fly ash and ground granulated blast-furnace slag, Cement and Concrete Composites 25 (3) (2003) 293–299.
[6] R. Birgul, Monitoring macro voids in mortar by X-ray computed tomography, Nuclear Instruments and Methods in Physics Research Section A: Accelerators, Spectrometers, Detectors and Associated Equipment 596 (3) (2008) 459–466.
[7] I. Odler, The BET-specific surface area of hydrated Portland cement and related materials, Cement and Concrete Research 33 (12) (2003) 2049–2056.
[8] H.M. Jennings, J.J. Thomas, A discussion of the paper "The BET-specific surface area of hydrated Portland cement and related materials" by Ivan Odler, Cement and Concrete Research 34 (10) (2004) 1959–1960.
[9] I. Odler, Reply to the discussion by H.M. Jennings and J.J. Thomas of the paper "The BET-specific surface area of hydrated Portland cement and related materials", Cement and Concrete Research 34 (10) (2004) 1961-1961.
[10] V. Baroghel-Bouny, Water vapour sorption experiments on hardened cementitious materials: Part I: Essential tool for analysis of hygral behaviour and its relation to pore structure, Cement and Concrete Research 37 (3) (2007) 414–437.
[11] S. Tada, K. Watanabe, Dynamic determination of sorption isotherm of cement based materials, Cement and Concrete Research 35 (12) (2005) 2271–2277.
[12] V. Baroghel-Bouny, Water vapour sorption experiments on hardened cementitious materials. Part II: Essential tool for assessment of transport properties and for durability prediction, Cement and Concrete Research 37 (3) (2007) 438–454.
[13] M.S. Ahs, Sorption scanning curves for hardened cementitious materials, Construction and Building Materials 22 (11) (2008) 2228–2234.
[14] A. Bilodeau, V.M. Malhotra, High-volume fly ash system: concrete solution for sustainable development, ACI Materials Journal 91 (1) (1997) 41–48.
[15] G. Baert. Physico-chemical interactions in Portland cement – (high volume) fly ash binders, PhD thesis, Ghent University, 2009 (ISBN: 978-90-8578-298-8).
[16] D.S. Klimesch, A. Ray, The use of DTA/TGA to study the effects of ground quartz with different surface areas in autoclaved cement: quartz pastes. Part 1: A method for evaluating DTA/TGA results, Thermochimica Acta 289 (1) (1996) 41–54.
[17] M.C. Garci Juenger, H.M. Jennings, The use of nitrogen adsorption to assess the microstructure of cement paste, Cement and Concrete Research 31 (6) (2001) 883–892.
[18] R.M. Espinosa, L. Franke, Influence of the age and drying process on pore structure and sorption isotherms of hardened cement paste, Cement and Concrete Research 36 (10) (2006) 1969–1984.
[19] E.P. Barrett, L.G. Joyner, P.P. Halenda, The determination of pore volume and area distributions in porous substances. I. Computations from nitrogen isotherms, Journal of the American Chemical Society 73 (1) (1951) 373–380.
[20] J. Hagymassy, S. Brunauer, R.S. Mikhail, Pore structure analysis by water vapor adsorption : I. *t*-curves for water vapor, Journal of Colloid and Interface Science 29 (3) (1969) 485–491.
[21] H.M. Jennings, Colloid model of C–S–H and implications to the problem of creep and shrinkage, Materials and structures 37 (2004) 59–70.
[22] R.F. Feldman, Helium flow characteristics of rewetted specimens of dried hydrated Portland cement paste, Cement and Concrete Research 3 (1973) 777–790.
[23] H.M. Jennings, Refinements to colloid model of C–S–H in cement: CM-II, Cement and concrete research 38 (2008) 275–289.
[24] H.M. Jennings, A model for the microstructure of calcium silicate hydrate in cement paste, Cement and Concrete Research 30 (1) (2000) 101–116.
[25] N. Yuasa, Sorption isotherm and moisture conductivity of cover concrete, Cement Science and Concrete Technology 52 (1998) 1042–1049 (in Japanese).
[26] J.J. Thomas, H.M. Jennings, A colloidal interpretation of chemical aging of the C–S–H gel and its effects on the properties of cement paste, Cement and Concrete Research 36 (1) (2006) 30–38.
[27] F. Roupuerol, J. Rouquerol, K. Sing, Adsorption by powders & porous solids, Academic Press, 1999.
[28] S. Brunauer, P.H. Emmett, E. Teller, Adsorption of gases in multimolecular layers, Journal of the American Chemical Society 60 (2) (1938) 309–319.
[29] R.A. Olson, H.M. Jennings, Estimation of C–S–H content in a blended cement paste using water adsorption, Cement and Concrete Research 31 (3) (2001) 351–356.